Polarimetric-Spatial Classification of SAR Images Based on the Fusion of Multiple Classifiers

Xiaoshuang Ma, Huanfeng Shen, *Member, IEEE*, Jie Yang, Liangpei Zhang, *Senior Member, IEEE*, and Pingxiang Li, *Member, IEEE*

***Abstract*—Traditional image classification methods are undertaken using the pixel as the research unit. These methods cannot use semantic information, and their classification results may not always be satisfactory. To solve this problem, objected-oriented methods have been widely investigated to classify remote sensing images. In this paper, we propose an innovative objected-oriented technique that combines pixel-based classification and a segmentation approach for the classification of polarimetric synthetic aperture radar (PolSAR) images. In the process of the pixel-based classification, a soft voting strategy is utilized to fuse multiple classifiers, which can, to some extent, overcome the drawback of majority voting. The experimental results are presented for two quad-polarimetric SAR images. The proposed classification scheme improves the classification accuracies after assembling the multiple classifiers, and provides the classification maps with more homogeneous regions by integrating the spatial information, when compared with pixel-based classification. By deploying multi-scale segmentation, we get a series of classification results, which again show that our method is superior to the conventional object-oriented methods.**

***Index Terms*—Object-oriented, polarimetric-spatial classification, polarimetric synthetic aperture radar, voting.**

I. Introduction

In many applications of remote sensing, the identification of the land-cover type by an image classification technique plays an important role. Remote sensing data obtained from different optical sensors have been commonly used to obtain land use and land cover (LULC) information. However, optical remote sensing is limited by weather conditions, and difficulties are often encountered in collecting timely LULC information. The synthetic aperture radar (SAR) system can provide a day-or-night, all-weather means of remote sensing and produces high-resolution images of the land under the illumination of radar beams. However, in the early years, many orbital SAR systems were single-polarization types and could result in confusion during the separation and mapping of LULC classes; this confusion stems from the limited information obtained by the single-polarization systems [1]. PolSAR is an advanced form of SAR, which focuses on emitting and receiving multi-frequency and fully polarized radar waves to characterize observed land-cover types and targets. Many researchers have shown that PolSAR has unique advantages in the classification of land-cover types [2]–[4].

Traditionally, the research unit for image classification has been the pixel. Many pixel-based algorithms have been developed for the supervised and unsupervised classification of PolSAR images in the last two decades. They can be divided into three major categories [5]: 1) the first type of algorithm is mainly based on the statistical characteristics of PolSAR images [6], [7]; 2) the second type of approach focuses on analyzing the polarimetric scattering mechanisms, which has the advantage that some prior information about the class types is provided [8], [9]; and 3) in the third category, both the analyses of the scattering mechanisms and the statistical information are combined [10]–[12]. Although the results of these pixel-based classification methods are generally positive, they still have some drawbacks. The main shortcoming is that they cannot use semantic information (texture, shape, etc.), except for remotely sensed information, which may lead to unsatisfactory classification results in some cases, especially for high-resolution images [13].

To solve this problem, objected-oriented classification methods have been developed. This methodology is implemented at the level of image objects, and uses the property and the relationship of objects to classify an image. Image objects correspond to geographic entities of the real world, and each entity is composed of pixels with the same characteristics [14]. In recent years, numerous object-oriented methods have been developed to classify SAR images [15]–[17], and they have achieved noticeable improvements in classification accuracy over the pixel-based methods. To sum up, in these traditional methods, classification is carried out at the level of image objects, using the mean value of all the pixels in a region as a representation of the object.

Another approach to improving classification accuracy is to fuse or combine multiple classifiers. The traditional approach for a pattern recognition problem is to search for the best individual classification algorithm. However, according to a large

Manuscript received February 20, 2013; revised April 21, 2013; accepted May 23, 2013. Date of publication June 20, 2013; date of current version March 14, 2014. This work was supported in part by the National High Technology Research and Development Program (863) under Grant 2011AA120404 and Grant 2013AA12A301, the Program for Changjiang Scholars and Innovative Research Team in University (IRT1278) under Grant 41271376, and by the Program for Changjiang Scholars and Innovative Research Team in University (IRT1278). *(Corresponding author: H. Shen.)*

X. Ma and H. Shen are with the Department of Resource and Environmental Sciences, Wuhan University, Wuhan, China (e-mail: mxs.88@whu.edu.cn; shenhf@whu.edu.cn).

J. Yang, L. Zhang, and P. Li are with the State Key Laboratory of Information Engineering in Surveying, Mapping and Remote Sensing, Wuhan University, Wuhan, China (e-mail: yangjie@lmars.whu.edu.cn; zlp62@lmars.whu.edu.cn; pxli@lmars.whu.edu.cn).

Color versions of one or more of the figures in this paper are available online at http://ieeexplore.ieee.org.

Digital Object Identifier 10.1109/JSTARS.2013.2265331

number of studies, there is no single algorithm that performs perfectly in classification, and each classifier has its own complementary benefits. Therefore, fusion strategies for multiple classifiers have been widely investigated, the aim of which is to determine an efficient combination that makes use of the complementary benefits of each classifier, while tackling the individual drawbacks, to improve the accuracy of the classification [18]. Classification ensemble methods can be categorized by the ways that they are built. Majority voting is a decision rule that selects one of the many alternatives, based on the predicted class with the most votes; it is easy to operate, and it is one of the most widely used ensemble methods for multiple classifiers [19], but its performance is sensitive to the precision of the base classifiers. Other ensemble strategies include Dempster-Shafer theory [20], statistical approaches [21], [22], Bayesian formulations [23], and neural networks [24].

In this paper, we propose a polarimetric-spatial classification method for SAR images, based on the fusion of multiple classifiers. First, a "soft voting" strategy, which can, to some extent, overcome the drawback of majority voting, is proposed for assembling the multiple pixel-based classifiers, and we get a class label for each pixel and a confidence coefficient of this class label. Second, we present an object-oriented method called "polarimetric-spatial classification" to combine the soft voting and segmentation results to classify the polarimetric SAR images. Within each image object, all the pixels are assigned to the class which has the highest weighted sum inside the region. Differing from the traditional object-based methods, the pixel-wise classification process that uses remotely sensed polarimetric information, and the segmentation process that uses contextual information, which are independent from each other in the proposed method, can take full advantage of both pixel-based analysis and object-based analysis.

The remainder of this paper is organized as follows. The proposed method is described in Section II. In Section III, the experimental classification results and analysis of two polarimetric SAR images are given. Finally, the conclusions are drawn in Section IV.

II. Methodology

This research aims at improving the classification accuracy for PolSAR images by combining the results of multiple classifiers with a segmentation approach. The whole processing chain (Fig. 1) consists of three major steps, as follows. Firstly, pixel-based classification of the preprocessed PolSAR data is implemented by three different classifiers, respectively, and a fused result is then obtained by soft voting. Secondly, independent of the pixel-based classification, the preprocessed image is segmented by a segmentation approach. Lastly, a polarimetric-spatial classification scheme is employed to get the final classification map, based on the fused result and the segmentation image.

A. Base Classifiers

In this study, we employ three base classifiers for the soft voting: Wishart classification, support vector machine (SVM) classification, and k-means classification. Wishart and SVM are supervised classifiers, and k-means is an unsupervised method.

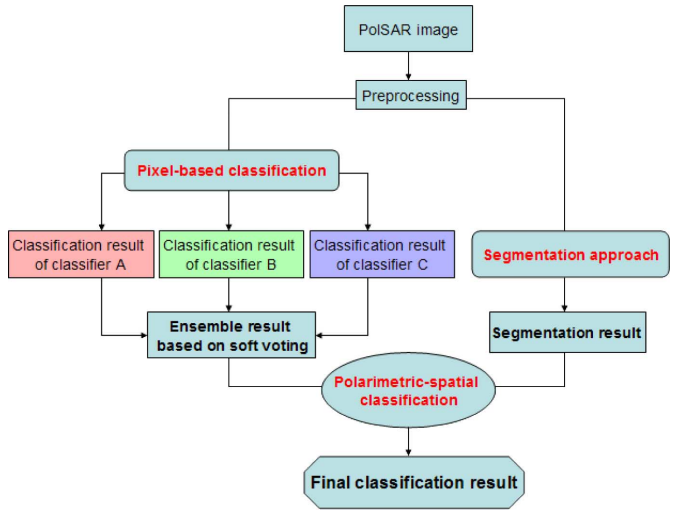

Fig. 1. Framework of the proposed polarimetric-spatial classification.

In general, the supervised classifiers can provide better classification results than the unsupervised classifiers; however, overclassification often happens in some homogeneous areas. The unsupervised classifiers can, however, effectively classify these spectrally homogeneous areas, and they are therefore a good supplement to the supervised classifiers [25].

1) Wishart Classification: For multilook PolSAR data represented in coherence or covariance matrices, Lee *et al.* [7] applied the principle of maximum likelihood to SAR and derived a Wishart distance to classify the PolSAR data. The main steps are as follows: initialize the pixel distribution over M clusters from the training data sets and get the center coherency matrix of each cluster. For the pixel p, p belongs to class ω_i if

$$\omega_i = \arg\min d\left([T]|\left[\hat{\sum}_i\right]\right) \tag{1}$$

where $d([T]|[\hat{\sum}_i]) = \ln|[\hat{\sum}_i]| + Tr([\hat{\sum}_i]^{-1}[T])$ is the so-called Wishart distance. $[T]$ is the coherency matrix of pixel, $[\hat{\sum}_i]$ is the center coherency matrix of the ith cluster, and $Tr(\bullet)$ denotes the trace of a matrix.

2) Support Vector Machine Classification: Support vector machine [26] is a machine learning method which uses a certain distance between samples as the criterion of classification, based on the principle of structural risk minimization. This method has been found to be a very efficient method for pattern recognition. In SVM classification for PolSAR data, the selection of the polarimetric indicators and the kernel function is an important step. In this paper, by testing different combinations of indicators, we select the nine elements of the coherency matrix and the H/A-alpha parameters of Cloude decomposition [27] as the polarimetric indicators for classification, and we choose the Gaussian radial basis function (RBF) with optimized parameters produced by PolSARpro software [28] as the kernel function.

3) K-Means Classification: K-means classification was proposed by Bezdek [29] and has become one of the most popular clustering methods to date. Wishart k-means clustering has been successfully applied to polarimetric SAR data [10], [11] and is

now considered to be a standard unsupervised classification approach. The k-means procedure is an iterative optimization algorithm, and is described in the following synopsis. First, initialize the pixel distribution over M clusters and compute the center coherency matrix of each cluster. For the pixel p, p belongs to class ω_i if

$$d\left([T]|\left[\hat{\sum}_i\right]\right) < d\left([T]|\left[\hat{\sum}_j\right]\right), \quad j=1,2,\ldots,M,\ j\neq i \tag{2}$$

where $d([T]|[\hat{\sum}_i])$ is the Wishart distance between pixel p and the center of the ith cluster. Then, for all the pixels in each class, updated class centers are derived and a new class assignment is performed. Lastly, if the algorithm meets the convergence criterion, output the result.

B. The Soft Voting Method for Multiple Classifiers

The majority voting rule derives from the hypothesis that the decision of a group is superior to that of the individual. In the principle of majority voting, if one pixel is identified as a class most frequently by the base classifiers, we give this class label to the pixel [30]. It is an easy-to-operate strategy for the fusion of multiple classifiers, because it does not assume prior knowledge of the behavior of the individual classifiers, and it does not require training with large quantities of representative recognition results [31]. However, this fusion scheme has a drawback in that each classifier has an equal influence on the final decision, which may adversely affect the classification efficiency of the classifier ensemble if some of the classifiers have low prediction accuracies for certain classes. The conflicting decisions made by these less reliable classifiers may influence the final decision, and thus overrule the decision made by the minority classifiers [32]. A more detailed analysis of majority voting can be found in [31].

In this present research, we employ a new approach called "soft voting" to fuse the base classifiers. The general flowchart of soft voting is given in Fig. 2. In our soft voting system, two principles are followed: the decision of the majority is superior to that of the individual; and a good classifier is superior to the relatively poor ones. According to many studies [33], the classification result of SVM will be superior to that of the maximum likelihood principle based classifiers if the elements of the coherency matrix and some other polarimetric parameters (entropy, span, etc.) are considered. Therefore, the SVM classifier can be considered as the decider when the three base classifiers have different opinions in the voting system. Meanwhile, considering the aforementioned drawback of the traditional majority voting rule, we introduce a confidence coefficient "R" to measure the reliability of the voting result of a certain pixel p. The soft voting process is described as follows: if the three base classifiers are unanimous in the class of p (i.e., without a decision conflict), assign p to this class, and set R_p as 3; if only two base classifiers have the same opinion as to the class of p, assign p to the class decided by the majority, and set R_p as 2; and if all of the base classifiers have different opinions as to the class of p, assign p to the class decided by the SVM classifier, and set R_p as 1. In other words, the higher the R_p is, the more reliable the voting result of pixel p is. Compared to the traditional majority voting method, the fusion result of our soft voting strategy is a union of class labels and their confidence coefficients. The use of R is further described in Section II-D.

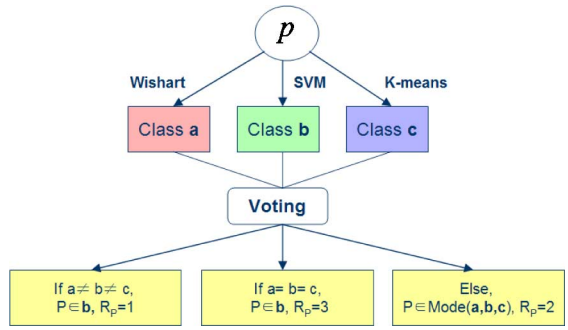

Fig. 2. Flowchart of the soft voting strategy.

C. Image Segmentation

To improve the classification results, the contextual information should be considered for incorporation into the classifiers. One approach to including spatial information in the classification consists of performing image segmentation. Many different segmentation approaches, such as SRM segmentation [34] and watershed segmentation [35], have been described in the published literature. In our study, we employ the fractal net evolution approach (FNEA) algorithm [36] as the segmentation means. This algorithm consecutively merges pixels or existing image objects. Essentially, the procedure identifies single image objects of one pixel in size and merges them with their neighbors, based on a relative homogeneity criterion. This homogeneity criterion measures how homogeneous or heterogeneous an image object is within itself, and consists of the homogeneity of the image feature information and the shape criteria [37].

1) Heterogeneity of the Image Feature Information: For a d-dimensional feature space, the heterogeneity of the image feature information h_a is described as follows:

$$h_a = \sqrt{\sum_d \left(\frac{f_{1d}-f_{2d}}{\sigma_{f_d}}\right)^2} \tag{3}$$

where f_{1d} and f_{2d} represent the dth feature values of two neighboring objects, respectively, and σ_{f_d} is the standard deviation of the dth feature.

2) Heterogeneity of the Shape Information: The heterogeneity criterion of the shape information consists of the smoothness heterogeneity h_s and the compactness heterogeneity h_c. They determine the smoothness and compactness of objects after merging, as follows:

$$h_s = \frac{l}{b} \tag{4}$$

$$h_c = \frac{l}{\sqrt{n}} \tag{5}$$

where l and n are the perimeter and pixel number of the object, respectively, and b is the area of the external rectangle of the object.

Giving a weight to each kind of heterogeneity, the total heterogeneity of the two adjacent objects is:

$$f = w_a h_a + w_{\text{shape}}(w_c h_c + w_s h_s) \tag{6}$$

where w_a, w_{shape}, w_c, and w_s represent the weights of the image feature heterogeneity, the shape heterogeneity, the smoothness heterogeneity, and the compactness heterogeneity, respectively. Finally, set a threshold to f and merge the two neighboring objects if the total heterogeneity of them does not surpass the threshold.

D. Polarimetric-Spatial Classification

As mentioned above, the pixel-based classification methods for PolSAR images mainly use the remotely sensed polarimetric information, and are greatly affected by speckle noise, which may sometimes lead to unsatisfactory classification results. Consequently, integration of the polarimetric and spatial information is often a good choice.

Unlike the conventional object-based schemes that classify images using segments as the process unit, a novel classification method was proposed to combine the pixel-based and spatial-based approaches for image classification in [38]. This method assigns all the pixels to the most frequent class inside an image object, which is the so-called "spectral-spatial classification." We refer the reader to [39] and [40] for more recent advances in the spectral-spatial classification of hyperspectral images. Although this methodology is designed for hyperspectral images, it is general and can be applied to other types of data as well [41]. Inspired by this, we propose a polarimetric-spatial classification scheme to integrate the polarimetric and spatial information for classification.

The scheme of polarimetric-spatial classification is displayed in Fig. 3. This figure is similar to the flowchart of the spectral-spatial classification scheme in [38], but the pixel-based classification result is obtained by soft voting, and a confidence coefficient is considered in the scheme. To begin with, three base classifiers—Wishart classification, SVM classification, and k-means classification—are utilized to classify the image, and their ensemble result is obtained by soft voting. In Fig. 3, the different colors refer to different class labels, and the numbers "1", "2", and "3" represent the confidence coefficient of each pixel. In the meantime, independent of the pixel-based classification, FNEA segmentation is also implemented on the original image, and "a", "b", and "c" are the object labels of the segmentation. Once the results of the above two approaches are obtained, they can then be integrated to accomplish an object-oriented classification. In the conventional schemes [38], [41], each pixel within an image object is considered to be of equal importance in determining the class of the segment. In this study, pixels are considered to be of varying importance, and we set the confidence coefficient R_p obtained by soft voting as the weight of pixel p in the polarimetric-spatial classification. As described in Section II-B, the higher the R_p is, the more reliable the voting result of pixel p is, and the more important pixel p is to determining the class of the segment. Finally, within each image object, all the pixels are assigned to the class which has the highest weighted sum inside the region. A mathematical model of this scheme is described as follows: inside an image object O, we can obtain the pixels that belong to a certain class ω_i and their confidence coefficients $R_{p\in\omega_i}$, and then all the pixels of this object are assigned to class ω_i, if

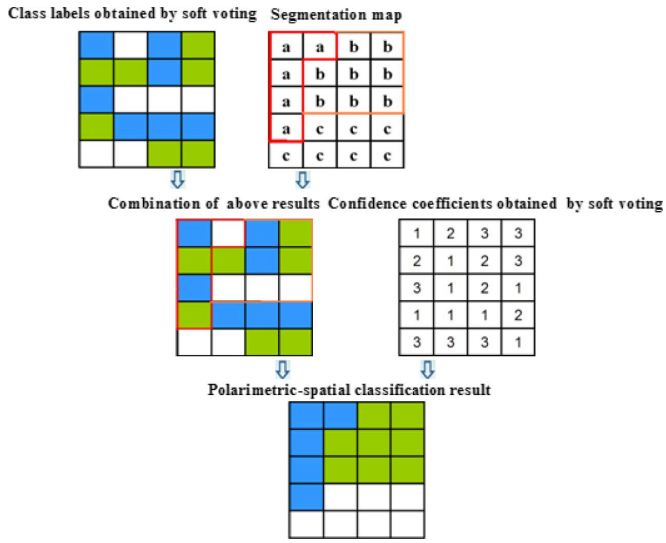

Fig. 3. The scheme for integrating the polarimetric and spatial information.

$$\omega_i = \arg\max sum\left(R_{p\in\omega_i}\right). \tag{7}$$

One point should be made clear. In our polarimetric-spatial classification, for a pixel p, when a decision conflict happens in the process of soft voting, only the class label decided by the majority, or the SVM classifier and its confidence coefficient, are considered. One may argue that, for each pixel, the classification results of all the classifiers should be considered and be involved in determining the class of the object. We found, however, that our method could achieve a better result if the classification results of the minority or relatively poor classifiers were discarded. Due to abandoning these unreliable classification results and considering the inequality of each pixel in an object, we alleviate the influence of the relatively poor classifiers, and ensure that the more reliable classifiers play a more important role in the polarimetric-spatial classification.

III. Experimental Results and Analysis

Two PolSAR data sets with different spatial resolutions are used for the experiments (Table I). The first data set, from Flevoland in the Netherlands, was acquired by the Airborne Synthetic Aperture Radar (AIRSAR) project of the National Aeronautics and Space Administration/Jet Propulsion Laboratory in 1989, and is distributed by the European Space Agency (ESA) as multilook processed data. The second data set was acquired by the X-Band Synthetic Aperture Radar (XSAR) airborne platform of the Thirty-Eighth Research Institute of the China Electronics Technology Group Corporation in 2011. Before the experiments, the refined Lee filter [42] was applied to the original data sets to reduce speckle noise, since it is

TABLE I
BASIC PARAMETERS OF THE DATA SETS

Data set	Platform	Polarization	Spatial resolution	Band	Number of looks
Flevoland	AIRSAR	Quad-polarization	10m*10m	L-Band	4-look
Haikou	XSAR	Quad-polarization	1m*1m	X-Band	1-look

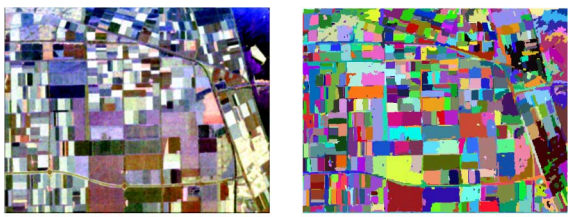

(a) (b)

Fig. 4. The Flevoland data set: (a) Pauli RGB image, and (b) the segmentation map.

able to preserve the polarimetric properties and the statistical correlations between channels.

A. Classification of the Flevoland Image

The image of Flevoland is a quad-polarimetric SAR data set. This L-Band data set was acquired by the AIRSAR airborne platform. Fig. 4 displays the Pauli RGB image of the data, which is formed with intensities of $|S_{HH} - S_{VV}|$ (red), $|S_{HV} + S_{VH}|$ (green), and $|S_{HH} + S_{VV}|$ (blue). By selecting the training samples of the image, we can obtain the initialization of the pixel distribution over the clusters for the supervised Wishart classification and the SVM classification. For the k-means classification, the initialization of the pixel distribution over the clusters is accomplished in a random way. The tested samples of each class are also selected to assess the classification performance in the following experiments. The image segmentation result of the FNEA algorithm is displayed in Fig. 4(b). In this paper, we choose the red-green-blue color components $(|S_{HH} - S_{VV}|, |S_{HV} + S_{VH}|, |S_{HH} + S_{VV}|)$ of the Puali RGB picture as the image features in the FNEA segmentation. The other parameters of segmentation are set as follows: $w_a = 0.9$, $w_{\text{shape}} = 0.1$, and $w_c = w_s = 0.5$. By setting different thresholds to the total heterogeneity f, multi-scale segmentation can be realized. In this experiment, by testing a series of segmentation scales, we set 50 as the best segmentation scale for the considered image, and obtain the optimal image segmentation result. The image, which previously consisted of pixels, is segmented into objects, and those continuous areas, which are the same physical class from a visual interpretation, are segmented into a few patches, which is more in line with reality. Compared with the pixel-based classification, the segmentation process considers more semantic/spatial information.

1) Polarimetric-Spatial Classification Results: Fig. 5 shows the classification results of the three base classifiers and their fusion results, and Tables II, III, and IV list the confusion matrices of the three base classifiers. Eleven categories of interest are considered, namely: C1, stem beans; C2, forest; C3, water; C4, potatoes; C5, Lucerne; C6, wheat; C7, bare soil; C8, beet; C9, rapeseed; C10, peas; and C11, grass (Fig. 5(a)).

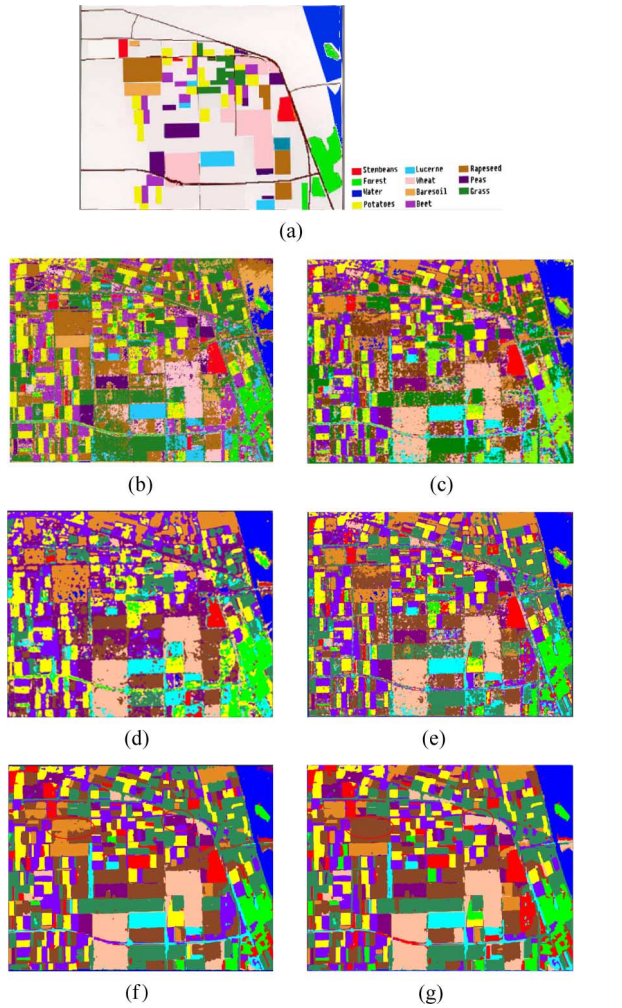

(a) (b) (c) (d) (e) (f) (g)

Fig. 5. Classification results of the Flevoland data set: (a) the ground truth map; (b) the Wishart classification result; (c) the SVM classification result; (d) the k-means classification result; (e) the majority voting result of multiple classifiers; (f) the P-S classification result based on traditional majority voting; and (g) the P-S classification result based on soft voting.

From Table II, we can see that the Wishart classification algorithm performs well in many aspects (Fig. 5(b)); however, some water pixels are misclassified as bare soil, which also have a weak back-scattering intensity. The cause of this problem may be that the distance measure of this algorithm is based largely on the value of the Pauli decomposition elements (diagonal elements of the coherency matrix) and, to a lesser extent, the off-diagonal matrix elements, which means that the assignment of pixels to clusters does depend on the SAR intensity [43]. The classification accuracy of wheat is also low, as reflected in Table II.

Table III indicates that SVM performs best among the three base classifiers, with a global accuracy (GA) of 84.0%, but misclassification between forest and potatoes, and rapeseed and bare soil still exists, which directly leads to the low user's accuracies of potatoes, bare soil, and rapeseed. As per the descriptions in [44] and [45], the procedure of applying SVM to SAR image classification is still uncertain, and how to select the optimum polarimetric indicators and optimize the kernel function of SVM for SAR data is still an open problem. In addition,

TABLE II
CONFUSION MATRIX FOR THE WISHART CLASSIFICATION OF THE FLEVOLAND DATA SET

	Sample pixels		Wishart classification											
	Train	Test	C1	C2	C3	C4	C5	C6	C7	C8	C9	C10	C11	User's accuracy (%)
Stem beans	420	455	445	0	0	4	0	6	0	0	0	0	0	97.8
Forest	551	818	12	776	0	17	13	0	0	0	0	0	0	94.9
Water	634	966	0	0	594	0	0	0	324	0	48	0	0	**61.5**
Potatoes	501	674	0	82	0	526	16	0	0	0	0	0	50	78.0
Lucerne	427	475	0	0	0	0	437	0	0	0	0	0	38	92.0
Wheat	646	1023	0	0	0	0	0	633	0	56	202	24	108	**61.9**
Bare soil	428	544	4	0	0	0	0	0	492	0	30	0	18	90.4
Beet	393	457	8	18	0	11	0	0	0	403	0	10	7	88.2
Rapeseed	515	741	16	0	0	0	0	31	0	5	684	0	5	92.3
Peas	446	690	0	2	0	3	22	0	0	31	10	622	0	90.1
Grass	384	499	33	20	0	11	28	3	0	0	0	0	404	81.0
Producer's accuracy (%)			86.0	86.4	100	92.0	84.7	94.1	60.3	81.4	70.2	94.8	64.1	Global accuracy (%)：81.9

TABLE III
CONFUSION MATRIX FOR THE SVM CLASSIFICATION OF THE FLEVOLAND DATA SET

	Sample pixels		SVM classification											
	Train	Test	C1	C2	C3	C4	C5	C6	C7	C8	C9	C10	C11	User's accuracy (%)
Stem beans	420	455	455	0	0	0	0	0	0	0	0	0	0	100.0
Forest	551	818	0	760	0	0	21	0	17	0	16	4	0	92.9
Water	634	966	0	0	911	22	0	0	33	0	0	0	0	94.3
Potatoes	501	674	0	244	0	421	0	0	0	0	0	0	9	**62.5**
Lucerne	427	475	0	0	0	0	390	0	0	0	0	0	85	82.1
Wheat	646	1023	0	25	0	18	0	907	0	11	52	10	0	88.7
Bare soil	428	544	0	0	131	0	0	0	373	0	40	0	0	**68.6**
Beet	393	457	0	0	0	0	0	21	0	387	32	0	17	84.7
Rapeseed	515	741	0	0	0	0	0	34	204	0	503	0	0	**67.9**
Peas	446	690	0	0	0	0	23	62	0	0	0	605	0	87.7
Grass	384	499	8	0	9	11	16	0	0	0	0	0	455	91.2
Producer's accuracy (%)			98.3	73.9	86.7	89.2	86.7	88.6	59.5	97.2	78.2	97.7	80.4	Global accuracy (%): 84.0

the number of support vectors sharply increases when the class number is large and the discrepancy between classes is small, which may degrade the performance of the SVM classifier.

For the k-means classification result, it can be clearly seen that there is severe misclassification between rapeseed and bare soil (Fig. 5(d)), and the classification results of some other classes, such as lucerne and beet, are also less reliable than the above two methods (Table IV), which results in a relatively low degree of GA. This problem can be ascribed to the shortcoming of the k-means classification in that the classification result of this algorithm is to some extent affected by the initial center of the clusters [46]. The initialization of the pixel distribution over the clusters in the present research is accomplished in a random way, which is not ideal, and therefore leads to this inefficiency.

The majority voting result (Fig. 5(e)) based on the above three classification methods is obtained. However, as shown in Table V, only a subtle advance in the classification accuracy of 0.8% is achieved after assembling the classifiers by majority voting, compared with SVM. This can be attributed to the shortcoming of the majority voting that we mentioned in Section II. Noting the low class-specific accuracies of potatoes, lucerne, and rapeseed, we find that these three classes have all been classified poorly by one or two of the base classifiers, without any exception. This phenomenon demonstrates the aforementioned view that, in the traditional majority voting rule, the conflicting decisions made by the less reliable classifiers may sometimes influence the final decision, and can overrule the decision made by the minority classifiers.

The polarimetric-spatial classification scheme is processed based on the ensemble result of multiple pixel-wise classifiers and the segmentation result. To begin with, we undertake an experiment for polarimetric-spatial classification based on traditional majority voting (Fig. 5(f)), i.e., without considering the confidence coefficient R of each pixel. From Table V, we can see that an advance in the classification accuracy of 3.7% is achieved after integrating the spatial information, compared with the majority voting result. In addition, as the segmentation process considers more spatial information, the object-oriented method provides the classification maps with more homogeneous regions, which is more in line with reality. This experiment shows that integrating spatial information by polarimetric-spatial classification can help to refine a pixel-based classification result.

Another phenomenon shown in Table V should also be pointed out: generally speaking, for polarimetric-spatial classification based on majority voting, the classification precision of a certain class is improved when the class obtained by majority voting has a relatively high class-specific accuracy; however, the classification precision of a certain class is decreased when the class obtained by majority voting has a relatively low class-specific accuracy, as with lucerne and rapeseed. This phenomenon indirectly validates that a relatively precise pixel-based classification result is necessary in polari-

TABLE IV
CONFUSION MATRIX FOR THE K-MEANS CLASSIFICATION OF THE FLEVOLAND DATA SET

	Test pixels	K-means classification											
		C1	C2	C3	C4	C5	C6	C7	C8	C9	C10	C11	User's accuracy (%)
Stem beans	455	436	0	0	0	11	0	0	0	0	0	8	95.8
Forest	818	6	724	0	81	7	0	0	0	0	0	0	88.5
Water	966	0	4	940	0	0	0	22	0	0	0	0	97.3
Potatoes	674	0	41	0	603	18	0	0	0	0	0	12	89.5
Lucerne	475	128	0	0	0	316	0	0	15	0	0	16	**66.5**
Wheat	1023	0	0	0	0	0	887	0	0	120	16	0	86.7
Bare soil	544	0	0	125	0	0	0	359	29	0	31	0	**66.0**
Beet	457	0	0	0	53	10	13	0	320	61	0	0	70.0
Rapeseed	741	0	0	8	0	0	0	443	0	270	0	20	**36.4**
Peas	690	0	0	0	0	89	0	0	15	44	542	0	78.6
Grass	499	5	0	0	20	61	0	0	10	0	0	403	80.8
Producer's accuracy (%)		75.8	94.1	87.6	79.7	61.7	98.6	43.6	82.3	54.5	92.0	87.8	Global accuracy (%): 79.0

metric-spatial classification. For the current research, an ideal segmentation algorithm is supposed to obtain image objects without under-segmentation, and mild over-segmentation is not a major problem, since the final goal is not to obtain the segmentation result but to classify the image. Thus, we are searching for the spatial regions of pixels that belong to the same physical object class. In such a case, if the classification results of pixels inside an image segment are not reliable enough, misclassification of all the pixels in this object will happen when integrating the spatial information by polarimetric-spatial classification, which will reduce the classification accuracy of that class.

After considering R, the classification result of polarimetric-spatial classification based on soft voting is obtained (Fig. 5(g)). As revealed in Table V, a further improvement in the GA of 4.1% is achieved, and some image objects belonging to wheat and rapeseed (marked by the red ellipses in the figure), which were misclassified in the last experiment, are classified correctly. This improvement is due to the fact that we consider the reliability or the weight of the voting result of pixels in the polarimetric-spatial classification, thus mitigating the influence of the less reliable classifiers. This experiment validates that, by employing the soft voting strategy, our method can get a better result.

2) A Comparison Between Polarimetric-Spatial Classification and Other Object-Oriented Methods: To further validate the advantage of our method, we also undertake a group of experiments to compare polarimetric-spatial classification with other object-oriented schemes. The first experiment is conducted to compare our method with conventional object-oriented methods, which classify the image using the segment as the process unit, and use the mean value of all the pixels in a region as a representation of the segment. In this experiment, an alternative way to accomplish the conventional object-oriented classification is to classify the image segments by the three base classifiers, respectively, and then combine the object-based classification results by majority voting. However, in practice, we found that the result of the aforementioned combination was even inferior to the object-based SVM classification result, since both the object-based Wishart classifier and the object-based k-means classifier had a poor classification performance. Thus, in this part, we choose the SVM classifier for classifying the image objects [16]. By setting a multi-scale for the segmentation, we get a series of classification accuracies for both polarimetric-spatial classification and object-oriented SVM classification, which are shown in Fig. 6.

The polarimetric-spatial classification achieves the optimal global accuracy, 92.6%, when the segmentation scale is set to 50; the object-oriented SVM classification achieves its optimal GA, 88.9%, when the segmentation scale is set to 90. This experiment verifies that our method is superior to the traditional object-based methods. It must be pointed out that a proper segmentation scale is important in object-oriented classification. As revealed in Fig. 6, the classification efficiency of both methods declines with the process of over-segmentation and under-segmentation. However, we have to face a dilemma, in that the automatic determination of the optimal segmentation scale is still a stern challenge for object-oriented classification.

Since the Flevoland image is a widely used agricultural data set for object-based classification, we conduct another experiment to compare our classification method with other published methods. This data set has several published ground truth maps, with different levels of detail and different category systems. In this part, we choose the work of Kaan Ersahin *et al.* [47], which is an object-oriented classification approach based on spectral graph partitioning for PolSAR data, to undertake a comparison. The results presented in [47] are obtained from a subset (200×320) of the Flevoland data set (Fig. 7(a)), and the ground truth map (Fig. 7(b)) from [47] consists of nine different land-cover types. To ensure the credibility of the polarimetric-spatial classification result, we re-collect the training samples for the two supervised base classifiers from areas outside of the subset. The global accuracies of the polarimetric-spatial classification and the spectral graph partitioning based classification are 87.5% and 81.2%, respectively, which clearly shows the superiority of our scheme.

B. Classification of the Haikou Image

The Haikou image is quad-polarimetric SAR data, which was obtained from an X-band airborne sensor, and the experimental results presented in this section are from a subset (311×391) of this data set. Fig. 8 displays the Pauli RGB image and the segmentation map of the data.

Fig. 9 shows the classification results. Five classes are considered: C1, grass land; C2, synthetic surface track; C3, house;

TABLE V
CLASSIFICATION ACCURACIES (%) FOR THE FLEVOLAND DATA SET

Class-specific accuracy	Wishart	SVM	K-means	Majority voting result	P-S classification based on majority voting	P-S classification based on soft voting
Stem beans	97.8	100.0	95.8	100	100	100
Forest	94.9	92.9	88.5	92.3	95.5	95.5
Water	**61.5**	94.3	97.3	96.6	98.2	100
Potatoes	78.0	**62.5**	89.5	**70.4**	99.3	99.3
Lucerne	92.0	82.1	**66.5**	**65.7**	**43.4**	**43.4**
Wheat	**61.9**	88.7	86.7	88.2	91.5	*98.0*
Bare soil	90.4	**68.6**	**66.0**	75.6	97.4	96.9
Beet	88.2	84.7	70.0	84.7	89.9	89.9
Rapeseed	92.3	**67.9**	**36.4**	**68.3**	**66.7**	*92.8*
Peas	90.1	87.7	78.6	89.9	82.8	85.9
Grass	81.0	91.2	80.8	94.2	100	100
Global accuracy	81.9	84.0	79.0	84.8	88.5	92.6

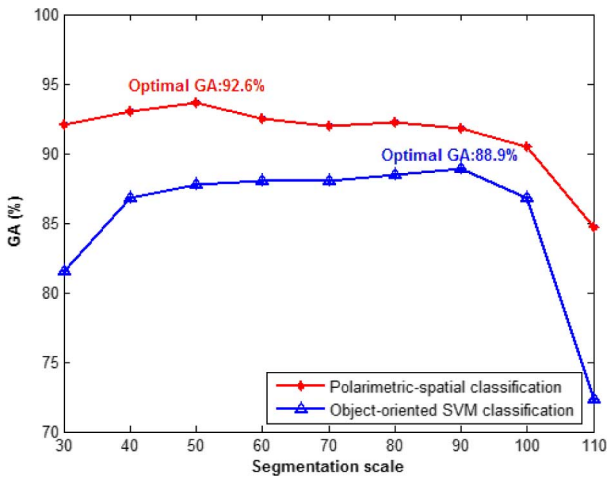

Fig. 6. The multi-scale classification results of the polarimetric-spatial classification and object-oriented SVM classification of the Flevoland data set.

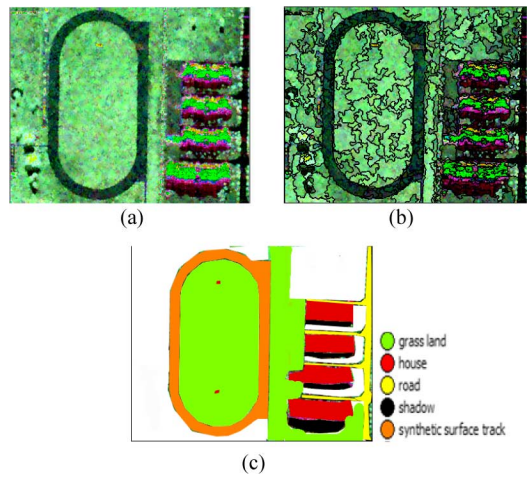

Fig. 8. The Haikou data set: (a) Pauli RGB image; (b) the segmentation map; and (c) the ground truth map.

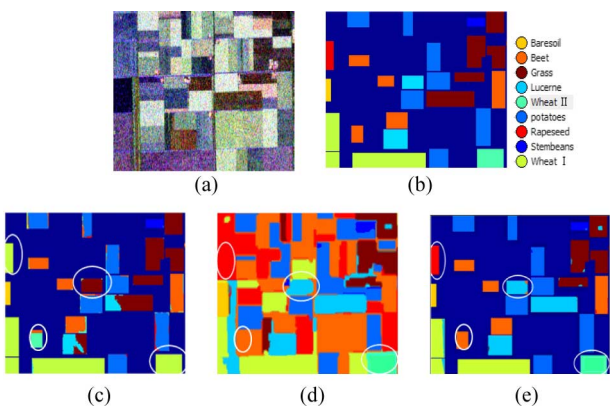

Fig. 7. Classification results of the Flevoland subset: (a) subset of the Flevoland data set; (b) ground truth map; (c) the classification result from [47]; (d) the classification result of the polarimetric-spatial classification method; and (e) the classification result with a void mask of (d).

C4, shadow; and C5, road. Table VI lists the classification accuracies for the Haikou data set.

We can see from Table VI that, among the three base classifiers, SVM (Fig. 9(b)) performs best, generally speaking, but does not perform very well when classifying the house class. The Wishart classifier (Fig. 9(a)) misclassifies many pixels of synthetic surface track that have a weak back-scattering intensity as road, for the reason we mentioned in the previous experiments, but it performs better with the house class than SVM. In general, the unsupervised classifiers can effectively classify the spectrally homogeneous areas; hence, k-means (Fig. 9(c)) yields a good classification performance on areas of the sports field, but it is still the most inferior classifier, with a GA of 73.2%, due to its imperfect initial center of clusters. After fusing these three classifiers, the majority voting result (Fig. 9(d)), which has an increase in accuracy of 1.5% over SVM, is obtained, and we get the R of each pixel in the soft voting process.

We also undertake a group of polarimetric-spatial classifications based on majority voting and soft voting. Their classification accuracies are 87.2% and 89.0%, respectively, which further demonstrates that, by employing the soft voting strategy, our method can get a better result, and a notable improvement in accuracy, ranging from 5.1% to 15.8%, is achieved, compared with the pixel-based methods.

By comparing the multi-scale classification results of polarimetric-spatial classification and object-oriented SVM classification (Fig. 10), we can see that, despite some fluctuations, the classification accuracies of the two methods show a downward trend with the process of over-segmentation and under-segmentation, which again verifies the significance of a proper segmentation scale, as with the last data set. Fig. 10 also shows that,

TABLE VI
CLASSIFICATION ACCURACIES (%) FOR THE HAIKOU DATA SET

Class-specific accuracy	Sample pixels		Wishart	SVM	K-means	Majority voting result	P-S classification based on majority voting	P-S classification based on soft voting
	Train	Test						
Grass land	420	1053	83.2	87.2	**70.2**	88.0	90.1	91.7
Synthetic surface track	398	708	**70.1**	89.0	98.9	80.6	92.7	95.3
House	354	717	88.8	**72.2**	91.4	87.4	87.9	89.4
Shadow	222	505	73.5	77.6	**3.6**	73.3	79.2	80.2
Road	307	536	88.2	82.6	86.8	85.3	84.1	84.1
Global accuracy			81.1	82.4	73.2	83.9	87.2	89.0

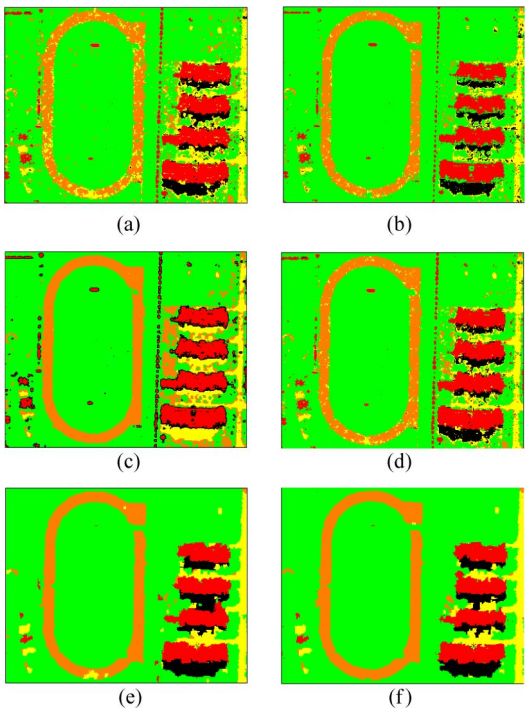

Fig. 9. Classification results for the Haikou data set: (a) Wishart classification; (b) SVM; (c) k-means; (d) the majority voting result of the multiple classifiers; (e) P-S classification based on traditional majority voting; and (f) P-S classification based on soft voting.

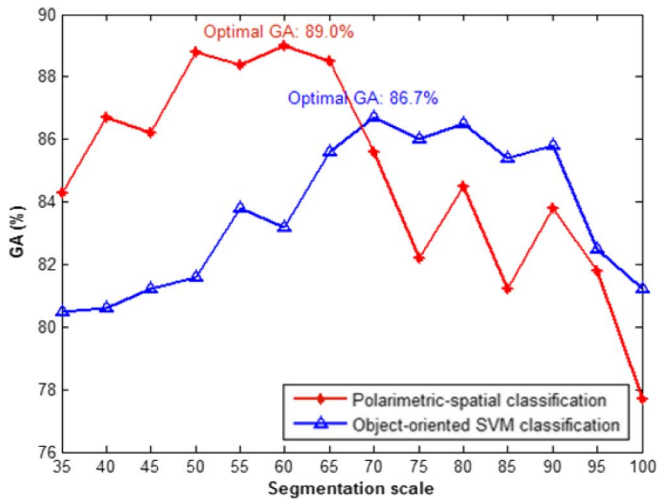

Fig. 10. The multi-scale classification results of the polarimetric-spatial classification and the object-oriented SVM classification of the Haikou data set.

for this data set, excessive over-segmentation and under-segmentation severely corrupts the classification accuracies, and these two methods have different degrees of susceptibility to the segmentation scale. Therefore, a proper way of undertaking the comparison is that only the relatively high accuracies of each method in Fig. 10 are utilized to assess their classification performance. Our method, which is better than object-based SVM and has a higher optimal accuracy, once again shows its superiority.

IV. CONCLUSION

In this paper, an object-oriented classification technique that combines a pixel-based classification and a segmentation approach is presented. The innovation of our work is that we develop a soft voting strategy to assemble the multiple classifiers, and investigate a new technique called "polarimetric-spatial classification" for the classification of PolSAR images. By conducting experiments on two quad-polarimetric SAR images, it was found that our classification scheme resulted in classification maps with more homogeneous regions, and achieved higher classification accuracies than the pixel-based methods. Multi-scale classification results of the polarimetric-spatial scheme were obtained, and comparisons of our method and other object-oriented methods were made, which further verify the advantage of our method in the classification of PolSAR data. However, further parameter optimization may be required for the operational use of the technique. Our future work will focus on developing a more efficient segmentation algorithm for SAR data, and further investigation of the interactive connection between pixel-based classification and the segmentation process will be undertaken.

ACKNOWLEDGMENT

The authors would like to thank ESA for providing the PolSARpro software, NASA/JPL for providing the PolSAR test data from Flevoland, and the 38th Research Institute of the China Electronics Technology Group Corporation for providing the Haikou data set.

REFERENCES

[1] Z. X. Qi, A. G. Yeh, X. Li, and Z. Lin, "A novel algorithm for land use and land cover classification using RADARSAT-2 polarimetric SAR data," *Remote Sens. Environ.*, vol. 118, pp. 21–39, Dec. 2012.

[2] J. C. Souyris, C. Henry, and F. Adragna, "On the use of complex SAR image spectral analysis for target detection: Assessment of polarimetry," *IEEE Trans. Geosci. Remote Sens.*, vol. 41, no. 12, pp. 2725–2734, Dec. 2003.

[3] C. Liu and C. H. Gierull, "A new application for PolSAR imagery in the field of moving target indication/ship detection," *IEEE Trans. Geosci. Remote Sens.*, vol. 45, no. 11, pp. 3426–3436, Nov. 2007.

[4] J. S. Lee, M. R. Grunes, and E. Pottier, "Quantitative comparison of classification capability: Fully-polarimetric versus dual and single-polarization SAR," *IEEE Trans. Geosci. Remote Sens.*, vol. 39, no. 11, pp. 2343–2351, Nov. 2001.

[5] B. Liu, H. Hu, H. Wang, K. Wang, X. Liu, and W. Yu, "Superpixel-based classification with an adaptive number of classes for Polarimetric SAR images," *IEEE Trans. Geosci. Remote Sens.*, vol. 51, no. 2, pp. 1–18, Feb. 2013.

[6] J. A. Kong, A. A. Swartz, H. A. Yueh, L. M. Novak, and R. T. Shin, "Identification of terrain cover using the optimum polarimetric classifier," *J. Electromagn. Waves Applicat.*, vol. 2, no. 2, pp. 171–194, 1988.

[7] J. S. Lee, M. R. Grunes, and R. Kwok, "Classification of multi-look polarimetric SAR imagery based on complex Wishart distribution," *Int. J. Remote Sens.*, vol. 15, no. 11, pp. 2299–2311, 1994.

[8] V. Zyl and J. Jakob, "Unsupervised classification of scattering behavior using radar polarimetry data," *IEEE Trans. Geosci. Remote Sens.*, vol. 27, no. 1, pp. 36–45, Jan. 1989.

[9] S. R. Cloude and E. Pottier, "An entropy based classification scheme for land applications of polarimetric SAR," *IEEE Trans. Geosci. Remote Sens.*, vol. 35, no. 1, pp. 68–78, Jan. 1997.

[10] J. S. Lee, M. R. Grunes, T. L. Ainsworth, L.-J. Du, D. L. Schuler, and S. R. Cloude, "Unsupervised classification using polarimetric decomposition and the complex Wishart classifier," *IEEE Trans. Geosci. Remote Sens.*, vol. 37, no. 5, pp. 2249–2258, Sep. 1999.

[11] L. Ferro-Famil, E. Pottier, and J.-S. Lee, "Unsupervised classification of multifrequency and fully polarimetric SAR images based on the H/A/Alpha Wishart classifier," *IEEE Trans. Geosci. Remote Sens.*, vol. 39, no. 11, pp. 2332–2342, Nov. 2001.

[12] J. S. Lee, M. R. Grunes, E. Pottier, and L. Ferro-Famil, "Unsupervised terrain classification preserving polarimetric scattering characteristics," *IEEE Trans. Geosci. Remote Sens.*, vol. 42, no. 4, pp. 722–731, Apr. 2004.

[13] J. Zhu, X. Fan, H. Guo, C. Wang, J. Tan, and X. Du, "Information extraction from high-resolution SAR image with object-oriented method," in *6th ISDE*, 2010.

[14] T. Blaschke and G. J. Hay, "Object-oriented image analysis and scale-space: Theory and methods for modeling and evaluating multi-scale landscape structure," *Int. Archives Photogramm. Remote Sens.*, vol. 34, no. 4, pp. 22–29, 2001.

[15] U. Benz and E. Pottier, "Object based analysis of polarimetric SAR data in alpha-entropy-anisotropy decomposition using fuzzy classification by eCognition," *Proc. IEEE IGARSS*, vol. 3, pp. 1427–1429, 2011.

[16] H. T. Li, H. Y. Gu, Y. S. Han, and J. H. Yang, "Object-oriented classification of polarimetric SAR imagery based on statistical region merging and support vector machine," in *EORSA*, 2008, pp. 1–6.

[17] Y. Dong, A. K. Milne, and B. C. Forster, "Segmentation and classification of vegetated areas using polarimetric SAR image data," *IEEE Trans. Geosci. Remote Sens.*, vol. 39, no. 2, pp. 321–329, Feb. 2001.

[18] B. M. Steele, "Combining multiple classifiers: An application of using spatial and remote sensed information for land cover type mapping," *Remote Sens. Environ.*, vol. 74, no. 3, pp. 545–556, Dec. 2000.

[19] H. Kim, H. Kim, H. Moon, and H. Ahn, "A weight-adjusted voting algorithm for ensembles of classifiers," *J. Korean Statistical Soc.*, vol. 40, no. 4, pp. 437–449, Dec. 2011.

[20] F. Tupin, I. Bloch, and H. Maitre, "A first step toward automatic interpretation of SAR images using evidential fusion of several structure detectors," *IEEE Trans. Geosci. Remote Sens.*, vol. 37, no. 3, pp. 1327–1343, May 1999.

[21] J. Franke and E. Mandler, "A comparison of two approaches for combining the votes of cooperating classifiers," in *Proc. 11th Int. Conf. Pattern Recognition*, 1992, vol. 2, pp. 611–614.

[22] Y. S. Huang and C. Y. Suen, "An optimal method of combining multiple experts for the recognition of unconstrained handwritten numeral recognition," *Pattern Analysis and Machine Intelligence*, vol. 17, no. 1, pp. 90–94, 1995.

[23] L. Xu, A. Krzyzak, and C. Y. Suen, "Methods of combining multiple classifiers and their applications to handwriting recognition," *IEEE Trans. Syst., Man, Cybern.*, vol. 22, no. 3, pp. 418–435, May 1992.

[24] D. S. Lee and S. N. Srihari, "Handprinted digit recognition: A comparison of algorithms," in *Proc. 3rd Int. Workshop Frontiers Handwriting Recognition*, 1993, pp. 153–162.

[25] H. Yang, Q. Du, and B. Ma, "Decision fusion on supervised and unsupervised classifiers for hyperspectral imagery," *IEEE Trans. Geosci. Remote Sens.*, vol. 7, no. 4, pp. 875–879, Oct. 2010.

[26] V. Vapnik, *The Nature of Statistical Learning Theory*. New York, NY, USA: Springer-Verlag, 1995.

[27] S. R. Cloude and E. Pottier, "A review of target decomposition theorems in radar polarimetry," *IEEE Trans. Geosci. Remote Sens.*, vol. 34, no. 2, pp. 498–518, Mar. 1996.

[28] L. F. Fmail and E. Pottier, "The polarimetric SAR data processing and educational tool," *European Space Agency*, 2005.

[29] J. C. Bezdek, R. Ehrlich, and W. Full, "FCM: The fuzzy c-means clustering algorithm," *Comput. Geosci.*, vol. 10, no. 2, pp. 191–203, 1984.

[30] C. G. Li and G. F. Shao, "Combination multiclassifier for object-oriented classification of forest cover," *J. Nanjing Forestry Univ.*, vol. 34, pp. 74–79, 2010.

[31] L. Lam and C. Y. Suen, "Application of majority voting to pattern recognition: An analysis of its behavior and performance," *IEEE Trans. Syst., Man, Cybern.*, vol. 27, no. 5, pp. 553–568, Sep. 1997.

[32] A. Cheriyadat, L. M. Bruce, and A. Mathur, "Decision level fusion with best-bases for hyperspectral classification," in *IEEE Workshop Adv. Tech. Analysis Remotely Sensed Data*, 2003, pp. 399–406.

[33] S. Fukuda and H. Hirosawa, "Polarimetric SAR image classification using support vector machine," *IEICE Trans. Electronics*, vol. E84-C, pp. 1939–1945, 2001.

[34] E. A. Carvalho, D. M. Ushizima, F. N. S. Medeiros, C. I. O. Martins, R. C. P. Marques, and I. N. S. Oliveira, "SAR imagery segmentation by statistical region growing and hierarchical merging," *Digital Signal Process.*, vol. 20, no. 5, pp. 1365–1378, 2010.

[35] L. Vincent and P. Soille, "Watersheds in digital spaces: An efficient algorithm based on immersion simulations," *IEEE Trans. Pattern Analysis and Machine Intelligence*, vol. 13, no. 6, pp. 583–598, Jan. 1991.

[36] M. Baatz, "Ecognition: Object oriented image analysis, user guide," *Definiens Imaging GmbH*, 2001.

[37] U. C. Benz, P. Hofmann, G. Willhauck, I. Lingenfelder, and M. Heynen, "Multi-resolution, object-oriented fuzzy analysis of remote sensing data for GIS-ready information," *ISPRS J. Photogramm. Remote Sens.*, vol. 58, no. 3, pp. 239–258, 2004.

[38] Y. Tarabalka, J. Chanussot, J. A. Benediktsson, J. Angulo, and M. Fauvel, "Segmentation and classification of hyperspectral data using watershed," *Proc. IEEE IGARSS*, vol. 3, pp. 652–655, 2008.

[39] K. Bernard, Y. Tarabalka, J. Angulo, J. Chanussot, and J. A. Benediktsson, "Spectral-spatial classification of hyperspectral data based on a stochastic minimum spanning forest approach," *IEEE Trans. Image Process.*, vol. 21, no. 4, pp. 2008–2021, Apr. 2012.

[40] M. Fauvel, Y. Tarabalka, J. A. Benediktsson, J. Chanussot, and J. C. Tilton, "Advances in spectral-spatial classification of hyperspectral images," *Proc. IEEE*, vol. 101, no. 3, pp. 652–675, Mar. 2013.

[41] Y. Tarabalka, J. A. Benediktsson, and J. Chanussot, "Spectral-spatial classification of hyperspectral imagery based on partitional clustering techniques," *IEEE Trans. Geosci. Remote Sens.*, vol. 47, no. 8, pp. 2973–2987, Aug. 2009.

[42] J. S. Lee, M. R. Grunes, and G. D. Grandi, "Polarimetric SAR speckle filtering and its impact for terrain classification," *IEEE Trans. Geosci. Remote Sens.*, vol. 37, no. 5, pp. 2363–2373, Aug. 1999.

[43] D. K. Atwood, D. Small, and R. Gens, "Improving PolSAR land cover classification with radiometric correction of the coherency matrix," *IEEE J. Sel. Topics Appl. Earth Observ. Remote Sens.*, vol. 5, no. 3, pp. 848–856, Jun. 2012.

[44] S. Fukuda, R. Katagiri, and H. Hirosawa, "Unsupervised approach for polarimetric SAR image classification using support vector machines," in *Proc. IEEE IGARRS*, 2002, vol. 5, pp. 2599–2601.

[45] N. Cristianini and J. S. Taylor, *An Introduction to Support Vector Machines and Other Kernel-Based Learning Methods*. Cambridge, U.K.: Cambridge University Press, 2000.

[46] F. Robinson, A. Apon, D. Brewer, L. Dowdy, D. Hoffman, and B. Lu, "Initial starting point analysis for K-means clustering: A case study," in *Proc. ALAR 2006 Conf. Applied Research in Inform. Technol.*, 2006.

[47] K. Ersahin, I. G. Cumming, and R. K. Ward, "Segmentation and classification of polarimetric SAR data using spectral graph partitioning," *IEEE Trans. Geosci. Remote Sens.*, vol. 48, no. 1, pp. 164–174, Jan. 2010.

Xiaoshuang Ma received the B.S. degree in geographic information system from Hubei University, Wuhan, China, in 2011. He is currently working toward the Ph.D. degree at the School of Resource and Environmental Sciences, Wuhan University.

His research interests include synthetic aperture radar image interpretation (segmentation and classification) and SAR signal processing.

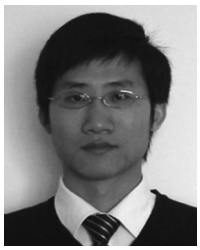

Huanfeng Shen (M'11) received the B.S. degree in engineering of surveying and mapping and the Ph.D. degree in photogrammetry and remote sensing from Wuhan University, Wuhan, China, in 2002 and 2007, respectively.

He served as a Research Assistant at the Department of Mathematics, Hong Kong Baptist University, Kowloon, Hong Kong, from 2006 to 2007. He is currently a Professor at the School of Resource and Environmental Sciences, Wuhan University. His research interests include image processing and fusion, remote sensing application, and global change. He has published more than 60 research papers. He has been supported by several talent programs, such as the New Century Excellent Talents by the Ministry of Education of China (2011) and Hubei Science Fund for Distinguished Young Scholars (2011).

Jie Yang received the Ph.D. degree from Wuhan University, China, in 2004.

Since 2011, he has held a Professor position with the State Key Laboratory of Information Engineering in Surveying, Mapping and Remote Sensing, Wuhan University. His main current research interests are in understanding SAR images.

Liangpei Zhang (M'06–SM'08) received the B.S. degree in physics from Hunan Normal University, Changsha, China, in 1982, the M.S. degree in optics from the Xi'an Institute of Optics and Precision Mechanics of Chinese Academy of Sciences, Xi'an, China, in 1988, and the Ph.D. degree in photogrammetry and remote sensing from Wuhan University, Wuhan, China, in 1998.

He is currently with the State Key Laboratory of Information Engineering in Surveying, Mapping and Remote Sensing, Wuhan University, as the Head of the Remote Sensing Division. He is a "Chang-Jiang Scholar" Chair Professor appointed by the Ministry of Education, China. He has more than 260 research papers and five patents. He is currently a Principal Scientist with the China State Key Basic Research Project from 2011 to 2016 appointed by the Ministry of National Science and Technology of China to lead the remote sensing program in China. His current research interests include hyperspectral remote sensing, high resolution remote sensing, image processing, and artificial intelligence.

Dr. Zhang serves as an Associate Editor of the IEEE TRANSACTIONS ON GEOSCIENCE AND REMOTE SENSING, the *International Journal of Ambient Computing and Intelligence*, the *International Journal of Image and Graphics*, the *International Journal of Digital Multimedia Broadcasting*, the *Journal of Geospatial Information Science*, and the *Journal of Remote Sensing*. He is an Executive member (Board of Governor) of the China National Committee of International Geosphere–Biosphere Programme, and Executive member for the China Society of Image and Graphics. He regularly serves as a Co-Chair of the series SPIE Conferences on Multispectral Image Processing and Pattern Recognition, Conference on Asia Remote Sensing, and many other conferences. He edits several conference proceedings, issues, and the Geoinformatics Symposiums.

Pingxiang Li (M'06) received the B.S., M.S., and Ph.D. degrees in photogrammetry and remote sensing from Wuhan University, Wuhan, China, in 1986, 1994, and 2003, respectively.

Since 2002, he has been a Professor with the State Key Laboratory of Information Engineering in Surveying, Mapping and Remote Sensing, Wuhan University. His research interests include photogrammetry and synthetic aperture radar image processing.